applied sciences

MDPI

Article

Mechanisms and Models of Attenuation of Shock Waves through Rock Formations

Shifan Zhao [1,2], Mingshi Gao [1,2,*], Dong Xu [1,2], Xin Yu [1,2] and Hongchao Zhao [3]

[1] School of Mines, China University of Mining and Technology, Xuzhou 221116, China
[2] The State Key Laboratory of Coal Resources and Safe Mining, China University of Mining and Technology, Xuzhou 221116, China
[3] School of Geology and Mining Engineering, Xinjiang University, Urumqi 830046, China
* Correspondence: cumt_gms@163.com; Tel.: +86-137-7599-8215

Abstract: Rock bursts have become one of the worst disasters in deep mines, and the safety of roadways is affected by stress waves generated when hard roofs fracture. Pictures of a mine site were collected using the Hujiahe mine as a case study. The damage characteristics of the roadway were analyzed and the damage process was reproduced using numerical simulation software. The attenuation characteristics of the strength of the shock wave as it passes from the impact shock source to the roadway are summarized. Based on the stress wave transmission mechanism and geological characteristics, a "shock wave attenuation model through rock formations" was established to analyze the transmission characteristics of impact stress under the composite roof structure. The strength criterion and energy balance equation for roadway damage under the action of shock waves are derived. This work provides a reference for roadway support under similar conditions and can be generalized and applied elsewhere.

Keywords: rock burst; roadway support; field research; numerical simulation; attenuation equation

check for updates

Citation: Zhao, S.; Gao, M.; Xu, D.; Yu, X.; Zhao, H. Mechanisms and Models of Attenuation of Shock Waves through Rock Formations. *Appl. Sci.* **2023**, *13*, 4526. https://doi.org/10.3390/app13074526

Academic Editor: Tiago Miranda

Received: 6 March 2023
Revised: 22 March 2023
Accepted: 23 March 2023
Published: 3 April 2023

Copyright: © 2023 by the authors. Licensee MDPI, Basel, Switzerland. This article is an open access article distributed under the terms and conditions of the Creative Commons Attribution (CC BY) license (https://creativecommons.org/licenses/by/4.0/).

1. Introduction

With the depletion of shallow coal, the depth of underground mines increases with time. The number of deep mines is increasing year by year. High stress, high permeability and high temperature have become important factors influencing production safety in deep mines [1]. High stress is an important factor in rock burst damage during mine production. In the event of a rock explosion, a violent high-energy shock wave is released from the source of vibration [2]. During its transmission and spread, the rock formations are damaged and fractures develop. Furthermore, the underground facilities are damaged [3]. Rock burst is different from sudden water, coal and gas protrusion and other disasters in mines; it is difficult to predict in advance, and the disaster occurs very quickly [4–6]. The energy from a mine earthquake can be quickly transmitted around the roadway and working face [7,8]. According to statistics, over 85% of rock burst damage occurs in the roadway, making the roadway a focus area for prevention and control. In recent years, domestic deep coal mines have been paying more and more attention to rock burst prediction and proposing many measures to prevent and control roadway areas [8,9], but rock burst control is still a substantial problem in deep mines [10].

Rock burst control around the roadway has become a difficult problem since the 20th century. Many scholars have proposed that the layout of the working face and the recovery roadway is an important condition influencing the extent of damage to the roadway in the case of rock burst [11,12]. However, coal and rock in the field are anisotropic in nature, unlike laboratory models. It is difficult to obtain a precise layout. Based on the historical distribution of mine earthquakes, it is possible to approximate the location of dynamic events in a mine. In reality, there are many mines that are not threatened by rock bursts in the early stages [13]. After a certain recovery period, they start to be affected by

frequent mine earthquakes. Based on the geological conditions of the mine, it is necessary to derive the effect of the dynamic wave on the roadway in the event of a rock burst by numerical simulation and equations [14,15].

In the last century, there were many scholars who tried to assess the process through theoretical calculation and computer simulation. The main focus has been on two areas: on the one hand, analysis of the level of energy released from the impact vibration source to measure the danger to the roadway [16], and n the other hand, the dynamic and static load stresses in the roadway have been studied, with increasing support strengths and decompression measures [17]. However, less research has been carried out in the area of rock burst stress wave attenuation. Dou et al. [18–20] described a strain-softening numerical model based on the Hoek–Brown failure criterion that was developed to evaluate the destressing efficiency of RDHB in selected underground coal mines. Ju et al. [21,22] proposed the concept of "high strength, strong pressure relief, and integrity" roadway support and the impact of "staggered peak pressure regulation + blasting top cut strong support" according to the violent and large-deformation characteristics of a rock burst in roadways. Pan et al. [23,24] established a mechanical model for rock burst to obtain critical indexes of the surrounding rock fracture and rock burst occurrence. The main influencing factors and laws of rock bursts were determined quantitatively. The numerical simulation of Kang et al. [25,26] demonstrated that the surrounding rock of the roadway underwent expansion and deformation, accompanied by redistribution of the surrounding rock stress due to the reinforcement of the roof and two sidewalls. Tan et al. proposed the "Stress Relief-support Reinforcement" synergistic technology for preventing a rock burst in deep roadways, studied the energy release mechanism of coal bodies and analyzed the failure characteristics and types of the surrounding rock due to different energy releases. Zheng et al. [27] Proposed that the roadway surrounding rock will collapse and lose stability in a large area under the roof cyclic dynamic load, and the ordinary supporting structure cannot fulfil its control function of the surrounding rock, resulting in the surrounding rock destruction and supporting structure failure. Zhang et al. [16] evaluated the abutment stress applied to the roadway surrounding rock by constructing an abutment stress transfer model after roadway excavation. Stress criterion and energy criterion for rock burst occurrence were proposed according to the three types of roadways.

In rock burst mines, the floor of the roadway often instantaneously rises violently, throwing off equipment and personnel in the roadway. The roof of the roadway tends to fall as a whole without extensive damage occurring [28,29]. In the roadway support system, the roof support is always in the primary position. A strong roof can produce a barrier effect on the roadway under static or dynamic stresses, reducing or preventing damage to the roadway [30,31]. In this paper, the stress conditions and strength criterion for roof damage under the action of shock waves and high stresses are investigated, taking the Hujiahe mine as an example. A shock wave attenuation model through the rock layer was established to analyze the bearing limit of the roadway roof in mine earthquakes and to study the energy balance criterion in the event of the rock burst.

Through the numerical simulation study of the 401,106 working face of the Hujiahe mine, a combined multi-level roof support was simulated in the event of a rock burst. The simulation results are combined with mathematical models. The results provide a theoretical basis for the stability control of the surrounding rock in the event of a rock burst.

2. Case Study

Geologic Conditions

The Hujiahe Coal Mine is a large underground mine in the northwest of Shaanxi Province. The mining area reaches 52 hectares. Figure 1 shows the location of the coal mine and the layout of the working face. The mine field is located in the middle of the Binchang mining area, with an altitude of about 1200 m. The Binchang mining area is located in the south of the Loess Plateau and the north of the Qinling Mountains. Affected by horizontal

stress, there are folds, faults and other special geological structures in the working face. The location of the mine is shown in Figure 1a.

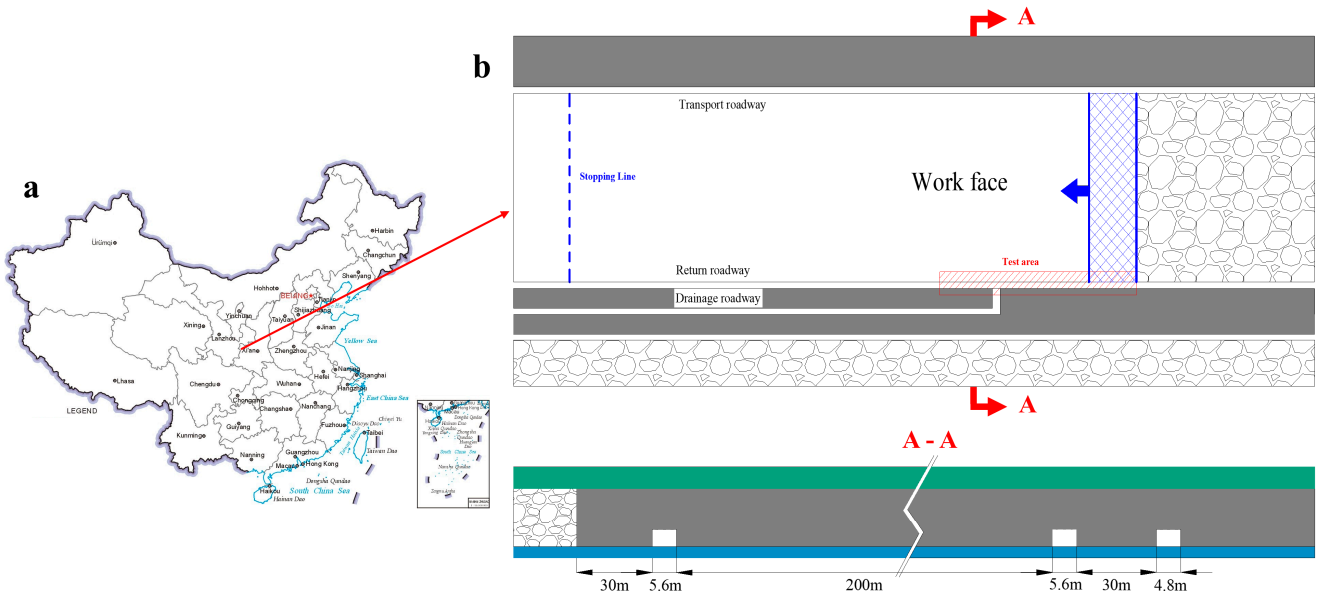


Figure 1. Mine location and working face layout. (**a**) Location of test site, (**b**) working face layout and cross section of test site.

The coal mine produces 6 million tons of coal annually. Currently, the working faces are 106 and 110 in the 401 mining area. The two working faces are very similar in terms of the layout and distribution of rock formations. The roadway is located in the bottom of the thick coal seam, and the thickness of the coal seam on the roof is 6 to 27 m, with an average of 23 m. A medium sandstone formation of approximately 36 m in thickness is present above the roof. The seismic sources are mainly close to the middle sandstone formation.

Figure 1b shows the layout of the working face and roadway. The working face is 200 m long with a recovery roadway along its length. The width of the recovery roadway is 5.6 m and the height is 3.7 m. The drainage roadway is on the right with a width of 4.8 m and height of 3.7 m. There is a 30 m coal pillar between the drainage roadway and the recovery roadway. The roof coal of the roadway is very thick. Therefore, the roof is extremely susceptible to collapse in a rock burst.

According to the mining conditions of the mine, it is a typical mine with high static stress and a thick coal roof. The roof-to-floor and the rib–rib displacement was measured in the mine's recovery roadway. Figure 2 shows the deformation characteristics of the roadway. The roof falling leads to bending of the steel belt, corner failure and floor heaving. Due to the timely cleaning of the roadway floor during recovery, no clear photographs were obtained. It can be seen that the displacement of the roof–floor of the roadway is much greater than that of the rib–rib, and the data collected were used to create a curve of the roadway deformation.

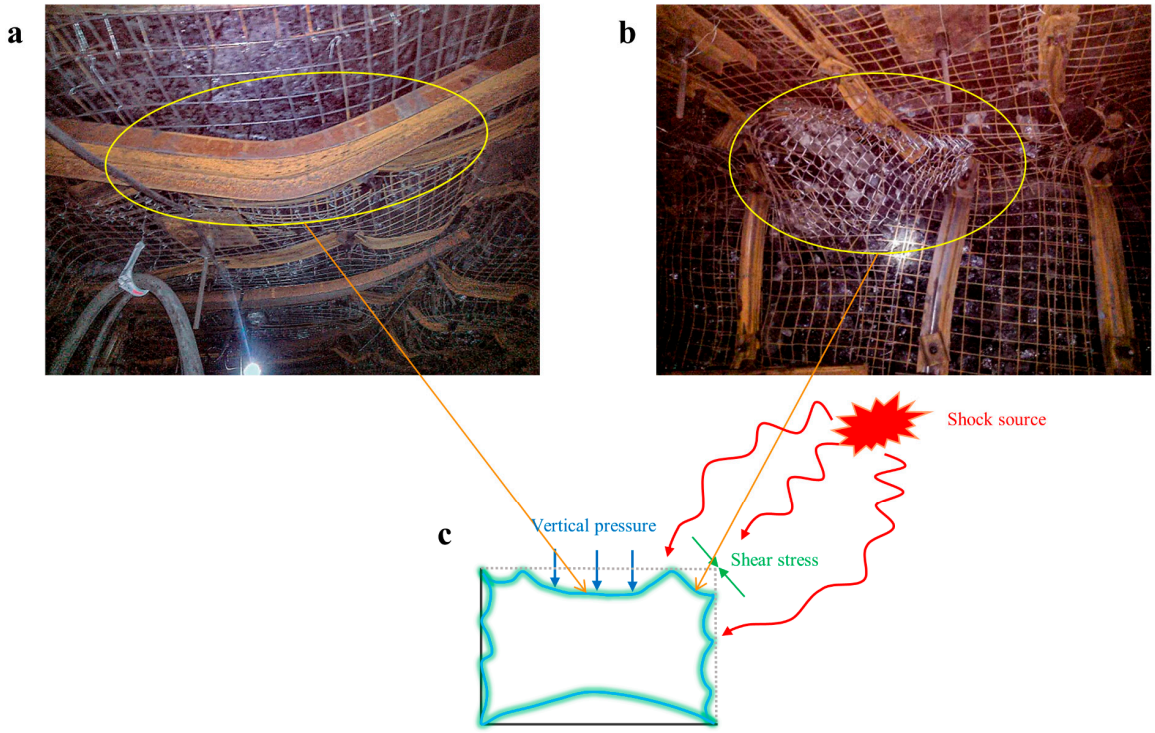


Figure 2. Damage characteristics of the roadway: (**a**) roof failure; (**b**) rib and corner damage; (**c**) roadway contour.

Figure 3 shows the deformation curves of the recovery roadway. Large deformations were generated in the area of 100 m distance in front of the coal wall as a result of recovery stresses and dynamic loading. The contraction of the roof–floor reached a maximum of 931 mm and the maximum displacement of the rib–rib was 543 mm, the former being 71.45% greater than the latter. Due to the influence of dynamic loads, the contraction of the roof and floor increases significantly in the range of 40 to 60 m, which shows that the control of the roof and floor of the roadway is the primary safety factor of the roadway.

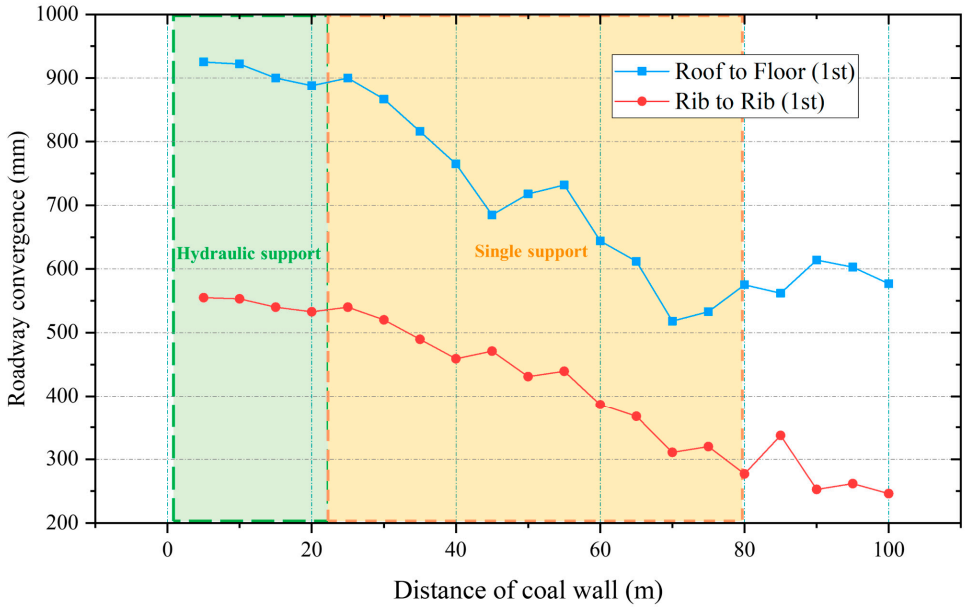


Figure 3. Roadway deformation curve.

3. Numerical Simulation Study

3.1. Model Building

The Universal Distinct Element Code (UDEC) is a common numerical simulation software for geotechnical engineering. The special calculation unit divides the material into blocks and presents a cloud of fracture and stress distribution in the blocks. In the numerical simulation of dynamics experiments, it is necessary to consider whether cracks are generated during the loading process.

According to the distribution characteristics of the working face and rock formation, the UDEC trigon numerical simulation model is established. A numerical model of the Hujiahe mine recovery area is shown in Figure 4, with the properties of each rock formation in the model on the right. The seven points from A to G in the figure represent the test points added to the model. The location of the impact shock source was set at the roof of the model based on the results of the field monitoring. The recovery roadway and drainage roadway are laid out on the coal seam floor. Table 1 shows the physical and mechanical parameters used for the mechanical analysis of each rock formation of the model.

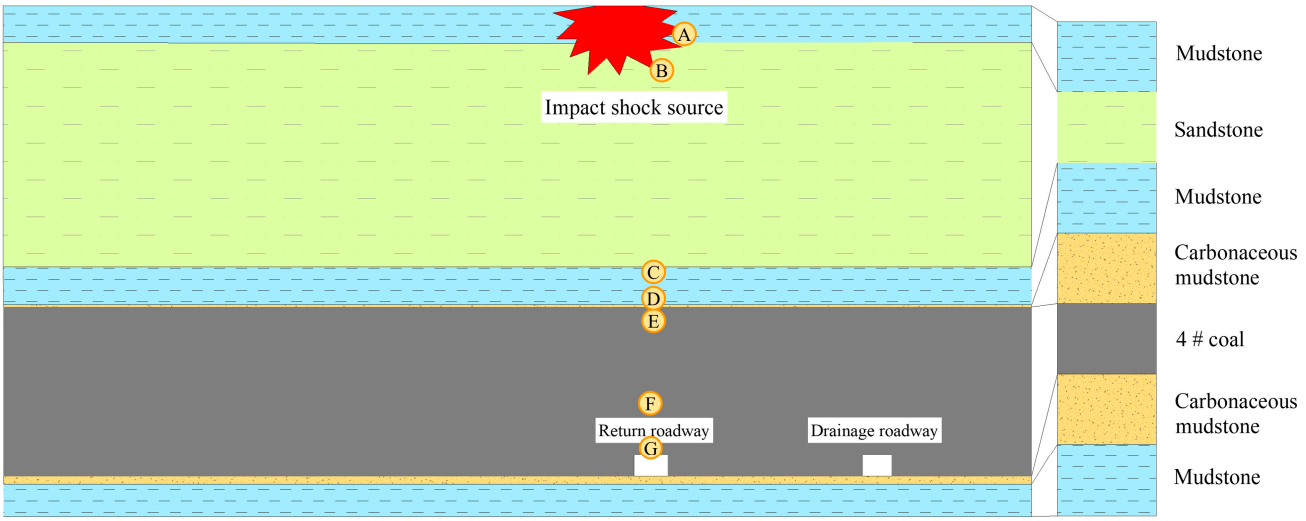


Figure 4. Numerical simulation model.

Table 1. Characteristics of the mechanical parameters of the coal rock mass.

Location	Lithology	Thickness (m)	Bulk (GPa)	Density (kg/m^3)	Shear (GPa)	Frictional Angle (°)	Cohesion (MPa)	Tension (MPa)
Roof	mudstone	5.58	15	2300	7	30	2	1.84
Main roof	sandstone	35.95	22	2600	14	39	10.2	1.2
Roof	mudstone	6.03	15	2300	7	30	2	1.84
Immediate roof	carbonaceous mudstone	0.45	15	2500	4	36	4.98	2.01
Coal seam	coal	23	10	1290	5	28	1.5	0.55
Immediate floor	carbonaceous mudstone	1.1	15	2500	4	36	4.98	2.01
Floor	mudstone	4.79	15	2300	7	30	2	1.84

Figure 5 shows the characteristics of the support construction arrangement for the recovery roadway. The support material is all anchor cable, with lengths of 3.5 m and 6.3 m, respectively. The longer anchor cables have a spacing and row spacing of 1600 mm and 1600 mm, respectively. Those of the other anchor cables are 800 mm and 800 mm. The two types of anchor cables are paired with a pallet made of 300 mm carbon steel and an M4-type steel belt, with 70 mm × φ6 mm metal mesh selected underneath the belt. The shock wave was set as a sine wave function with a peak of 100 MPa and a loading time of 0.2 s.

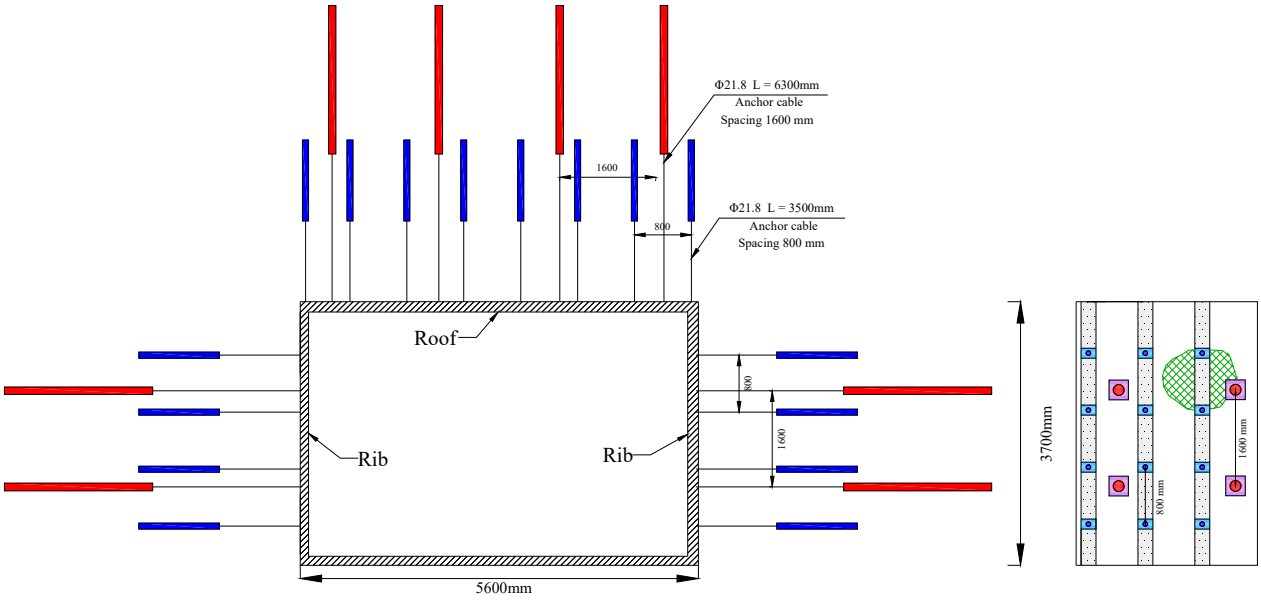


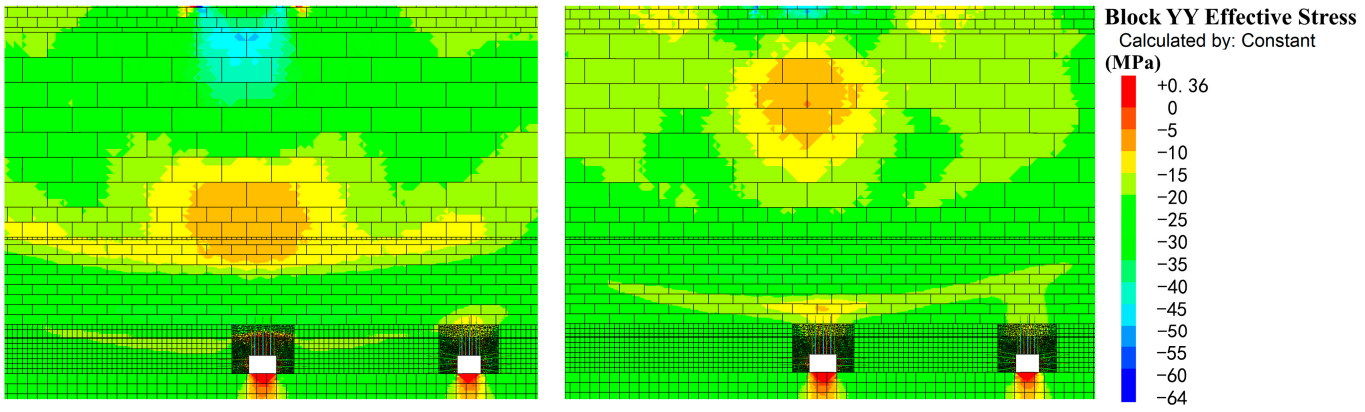
Figure 5. Roadway support parameters.

3.2. Results

The location of the impact shock source is above the recovery roadway. During this period, the shock wave is transmitted from the impact shock source through multiple rock formations to the roadway. The dynamic shock stress and the energy are significantly decaying. The destructiveness of the shock waves on the roadway is mainly caused by the impact dynamic stresses accumulated on the roadway static stresses, which overpower the strength of the surrounding rock. The transmission process and attenuation characteristics of the shock waves are shown in Figure 6.

As shown in Figure 6a–d, the peak stress decreased from 125 MPa to 40 MPa after the shock wave passed through the first mudstone layer. It decreased to 15 MPa after passing through the sandstone layer. After passing through the mudstone and roof coal, the vertical stresses were almost constant. For this reason, the stress characteristics of the different rock formations were recorded separately at different rock positions.

Figure 7 shows the curve of Y displacement at the monitoring points A to G. The Y displacement at the monitoring point from the source of the shock to the roadway envelope increases. The rate of decrease in the center of the oscillation increases for each curve. The velocity of the oscillation is the fastest at the source, but the change in displacement is the smallest.



(**a**) (**b**)

Figure 6. *Cont.*

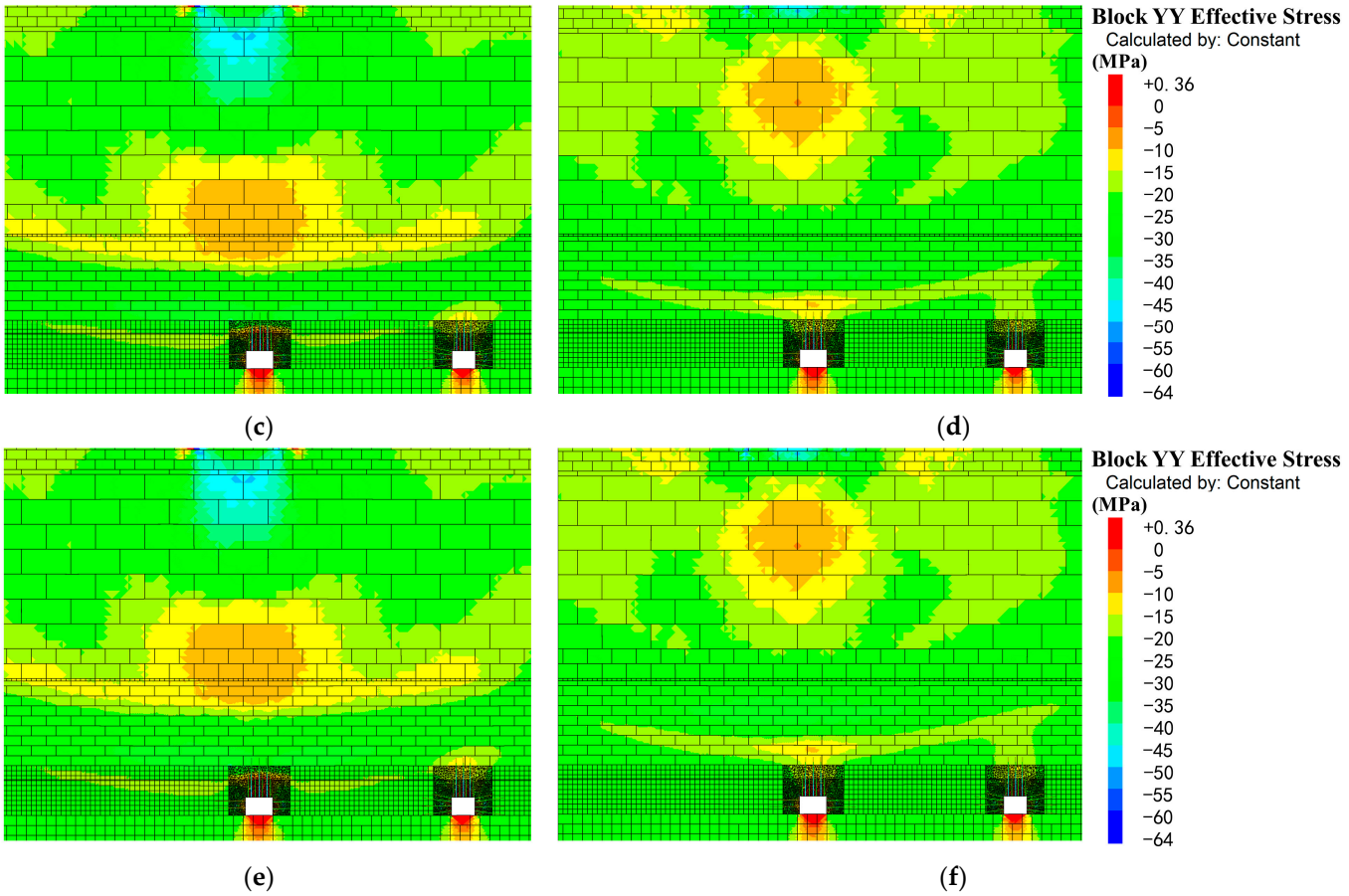


Figure 6. Block YY effective stress during dynamic simulation. (**a**–**f**) Represents a model of 2900, 3000, 3100, 3200, 3300, 3400 time steps, respectively.

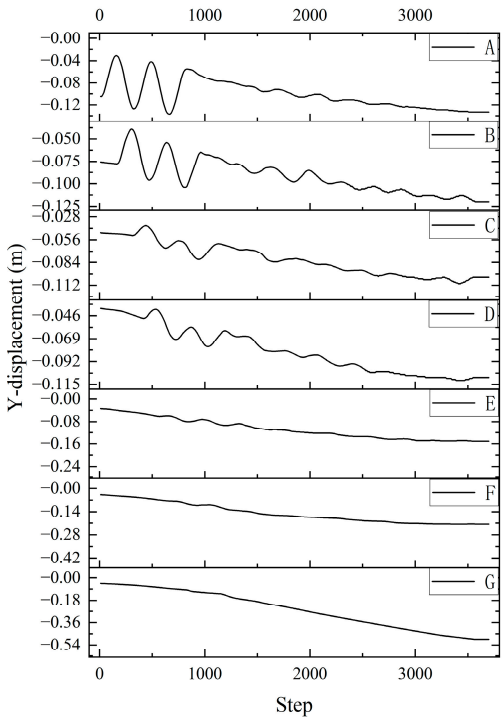


Figure 7. Y−displacement curve of monitoring point.

Figure 8 shows the vertical velocity and displacement curves monitored at the location of points A to G as the shock wave passes through each rock formation. The shock wave velocity shows a gradual attenuation from the source, with the greatest attenuation through the medium sandstone formation. The lower the distance to the roadway, the lower the oscillation amplitude of the wave velocity. The energy of the shock wave through this rock formation decays significantly. Sandstone and coal are the two sections with the greatest rate of change in displacement. Because of the free space such as the roadway and the working face, the fractures are constantly extended and have a greater vertical displacement towards the free space.

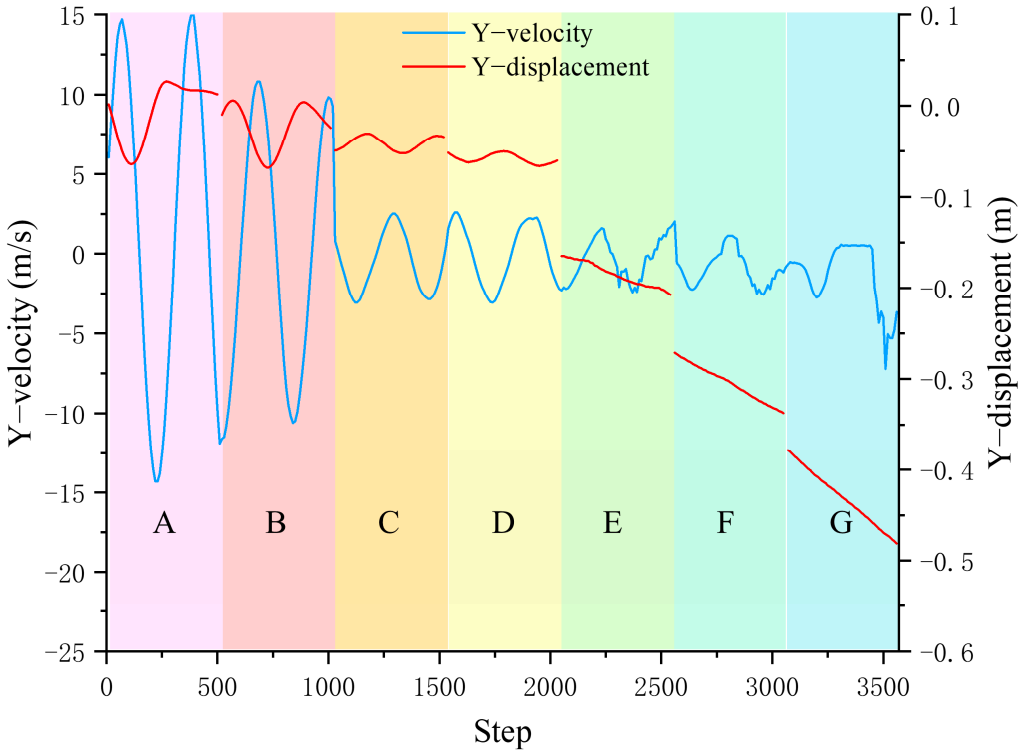


Figure 8. Y−velocity and Y−displacement curve of monitoring point.

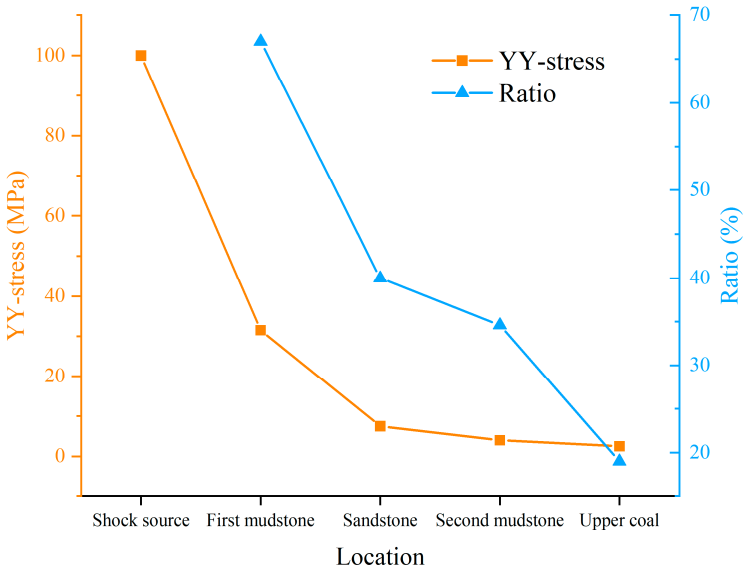


Figure 9. Stress decay curves.

Figure 9 shows the stress decay characteristics of the impact stress in the process of conduction. As seen in the process of stress transfer, the decay rate constantly slows down and tends to disappear. The decay rate during conduction is simply calculated using the following equation:

$$\eta = -log_{h_i}\left(\frac{\sigma_{h_i}}{\sigma_{h_{i-1}}}\right) \quad (1)$$

where η is the attenuation rate of the stress wave and σ_{h_i} is the vertical stress of the ith rock formation. The following conclusions can be drawn after carrying out calculations:

(1) There is a decreasing trend in the rate of attenuation during stress wave conduction.
(2) There is a large difference in the attenuation coefficients during the passage through rock formations of the same properties.
(3) The attenuation coefficients of the sandstone closer to the shock source are different from the second mudstone layer, which shows that different rock properties attenuate the shock waves to different degrees.

By the time the stress wave is transmitted to the second sandstone layer, it has attenuated to less than 10 MPa, at which point the rock layer and the roadway support system can withstand the damage caused by the stress shock wave.

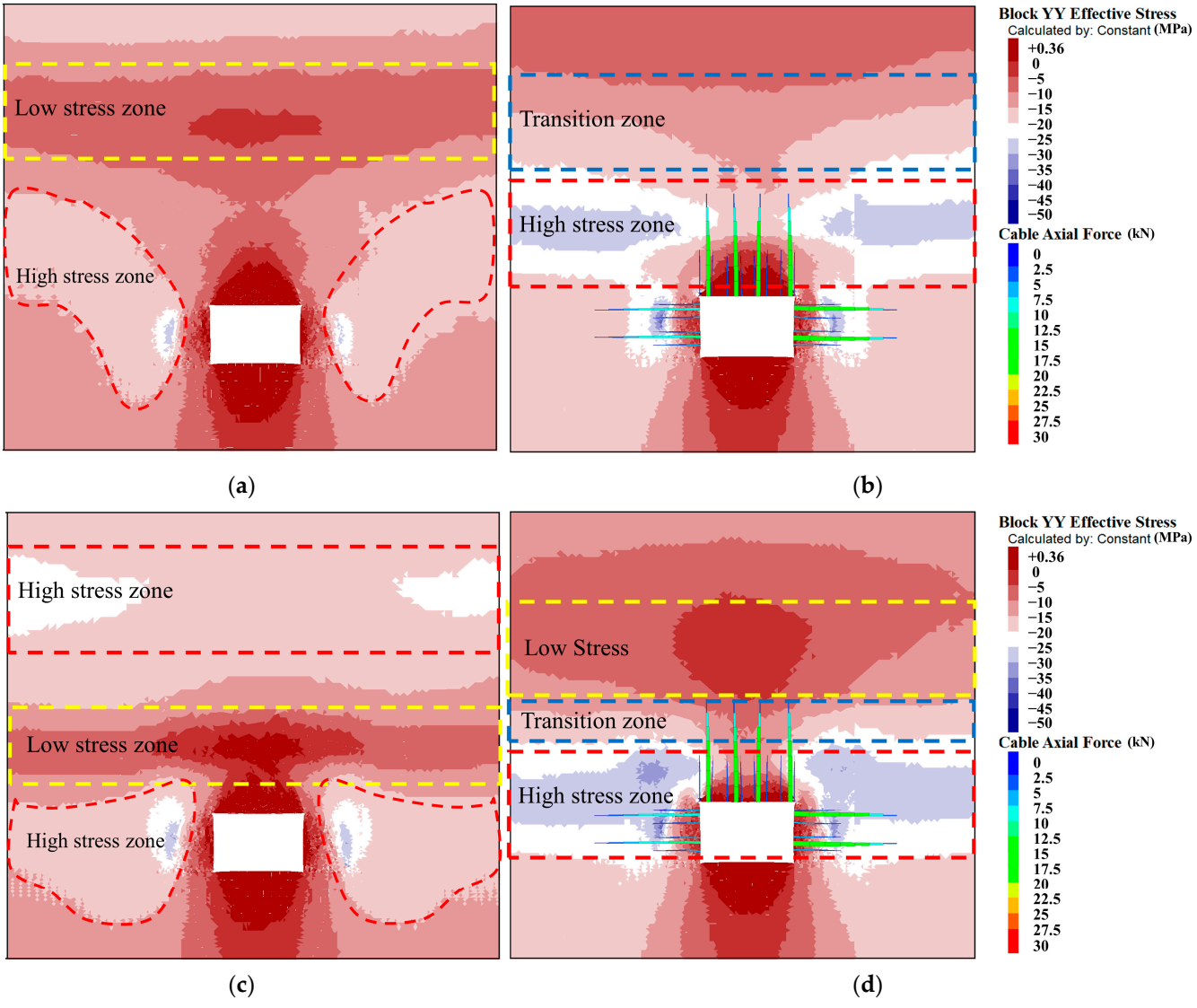
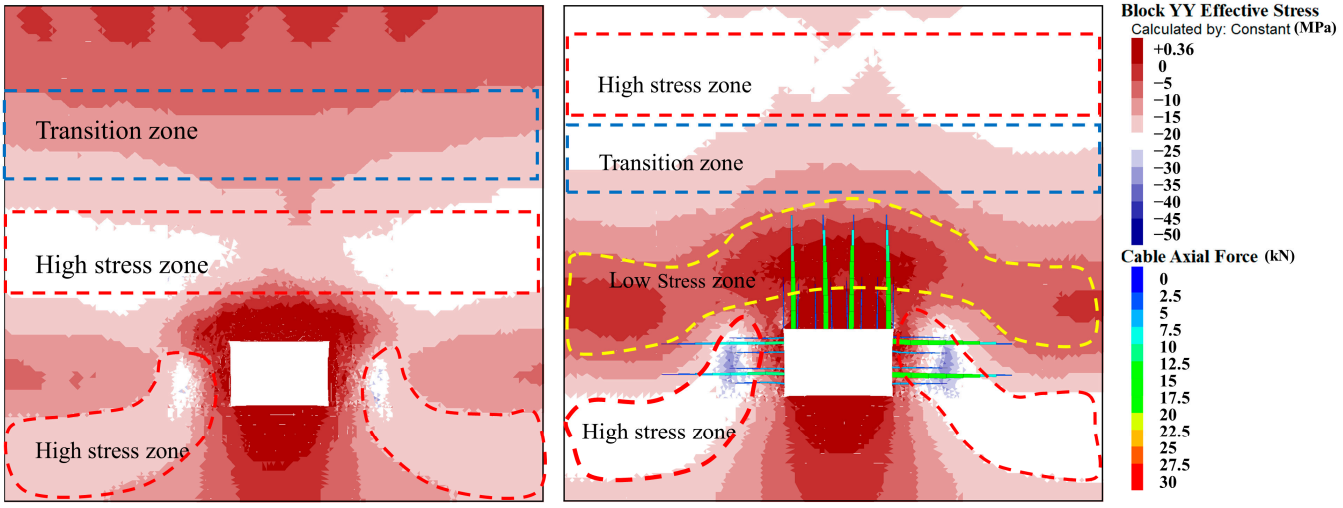


Figure 10. *Cont.*



(**e**) (**f**)

Figure 10. Shock wave YY−stress distribution characteristics through the roadway-surrounding rock. (**a**) The shock wave reaches the roadway roof (no support). (**b**) The shock wave reaches the roadway roof. (**c**) The shock wave reaches the two ribs of the roadway (no support). (**d**) The shock wave reaches the two ribs of the roadway (**e**) The shock wave reaches the floor of the roadway (no support) (**f**) The shock wave reaches the floor of the roadway.

Figure 10 shows the stress−YY characteristics of the shock wave passing through roadway. The figure shows the stress distribution around the roadway with the axial force characteristics of the anchor cable when the shock wave reaches the roof of the roadway, the two ribs of the roadway and the floor of the roadway, respectively. For the no-support model, during this process, the shock wave always accumulates with the static load on both ribs of the roadway, accelerating roadway damage. Under the influence of the support, the integrity of the roadway envelope is better, and no large deformations occur when the shock wave arrives, slowing the damage to the roadway. In brief:

(1) The axial force of the anchor cable remains almost unchanged during this process. It does not proactively change its own axial force to resist damage from the shock wave.
(2) The loose areas of the roadway in the no-support conditions are much greater than in supported structures.
(3) The support structures will reinforce the roadway, making it resist shock waves as intact rock would. They change the stress distribution around the roadway.

4. Discussion

4.1. Shock Wave Disturbance Roadway Mechanism

The mechanism of the dynamic and static load superposition of rock burst is still recognized by most scholars. This theory explains the cause of rock burst and summarizes the natural and artificial factors that affect the intensity of rock burst. Among the natural factors, special geological structure and a thick hard roof are the most common reasons. Among the human factors, unreasonable working face layout and unreasonable measures to reduce rock pressure will also greatly increase the probability of rock burst. For example, in the process of coal mining, the hard roof is difficult to break in the process of mining. When it breaks, it releases substantial impact energy. The resulting shock wave instantly damages or destroys the underground facilities. According to previous research:

(a) When the shock wave spreads from the source to the surrounding rock of the roadway, the intensity gradually decreases.
(b) There are different attenuation rates in rock formations with different properties.
(c) During the transmission of the shock wave, the trend of the attenuation rate is decreasing.

(d) Anchor cables cannot adaptively change their anchorage strength to stabilize the roof when the shock wave reaches the roadway. The role of the anchor cable is that it creates a complete structure with the roof of the roadway to resist shock waves.

Figure 11 shows the damage characteristics of a rock formation when a mining earthquake occurs in a hard roof. When the rock burst occurs in the roof, the energy is rapidly released and spread, with wide fractures spreading out from the source. The subsurface rock is intact and shock waves are easily transmitted from the source to the roadway-surrounding rock. Combined with the conclusions of Section 3:

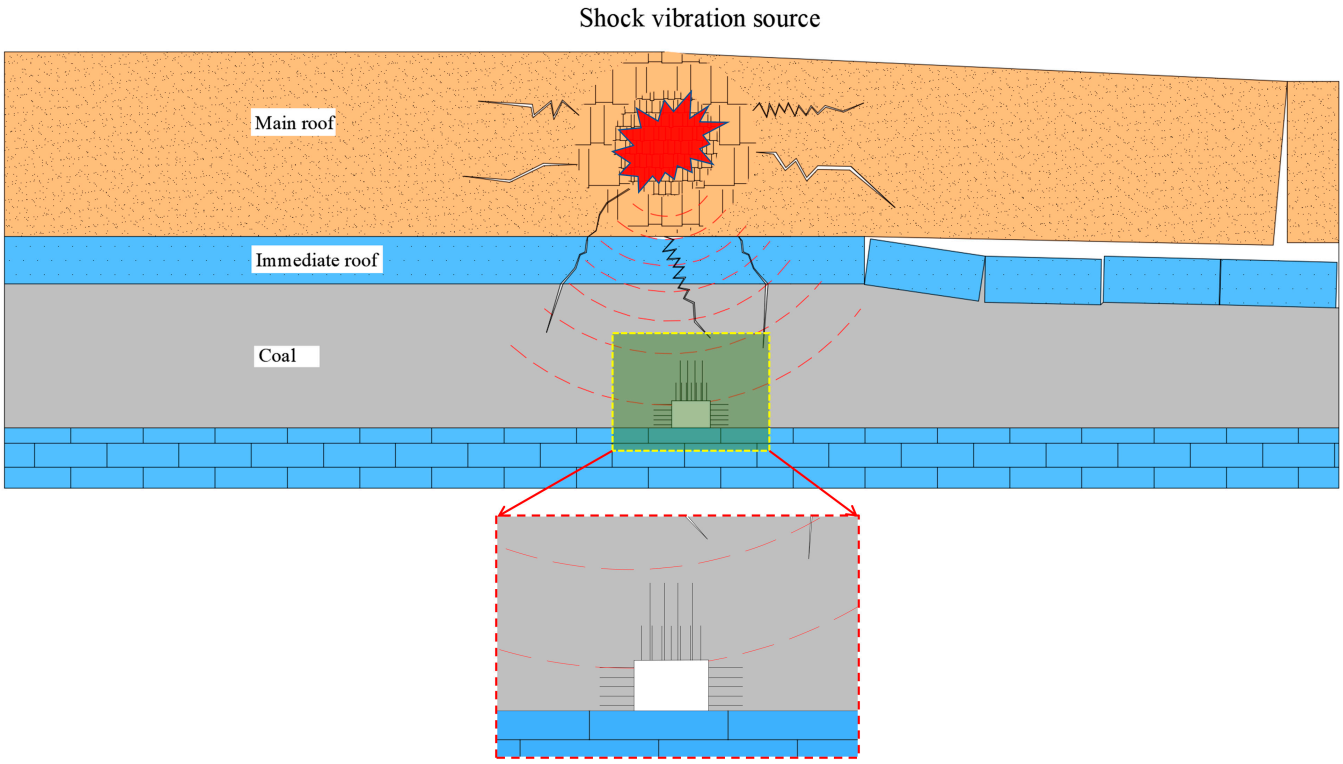


Figure 11. A model of shock wave transmission through rock formations.

(a) Due to the confines of the underground space, there is not enough space at the shock source for great displacements. The closer to the shock source, the higher the degree of damage to the rock.
(b) For dynamic rocks, the roadway is a perfect free space. The rock damage is also dramatic here.
(c) The subsidence of the roadway roof is an important factor in roadway damage.

In the rock burst, not all rock formations are damaged, and we have focused on the damage to the roadway-surrounding rock. There are many influencing factors, such as the energy generated by the rock burst, the location of the roadway relative to the impact shock source and the support measures for the roadway. Based on these factors and conditions, a "shock wave through-layer attenuation model" is established and the equation for the attenuation of shock waves during a rock burst is derived.

4.2. Model Establishment

As the location of the impact shock source is usually the location of the fracture in the hard roof, Figure 12 shows the transmission of impact energy through the rock formation to the roadway when the impact dynamic load occurs. Assuming that the impact source is located in the rock formation above the roof of the roadway, the transmission of the shock wave from the impact source to the roof of the roadway requires passing through n layers of rock in sequence, where the thickness of the rock formation is h_1, h_2 to h_n, in that order.

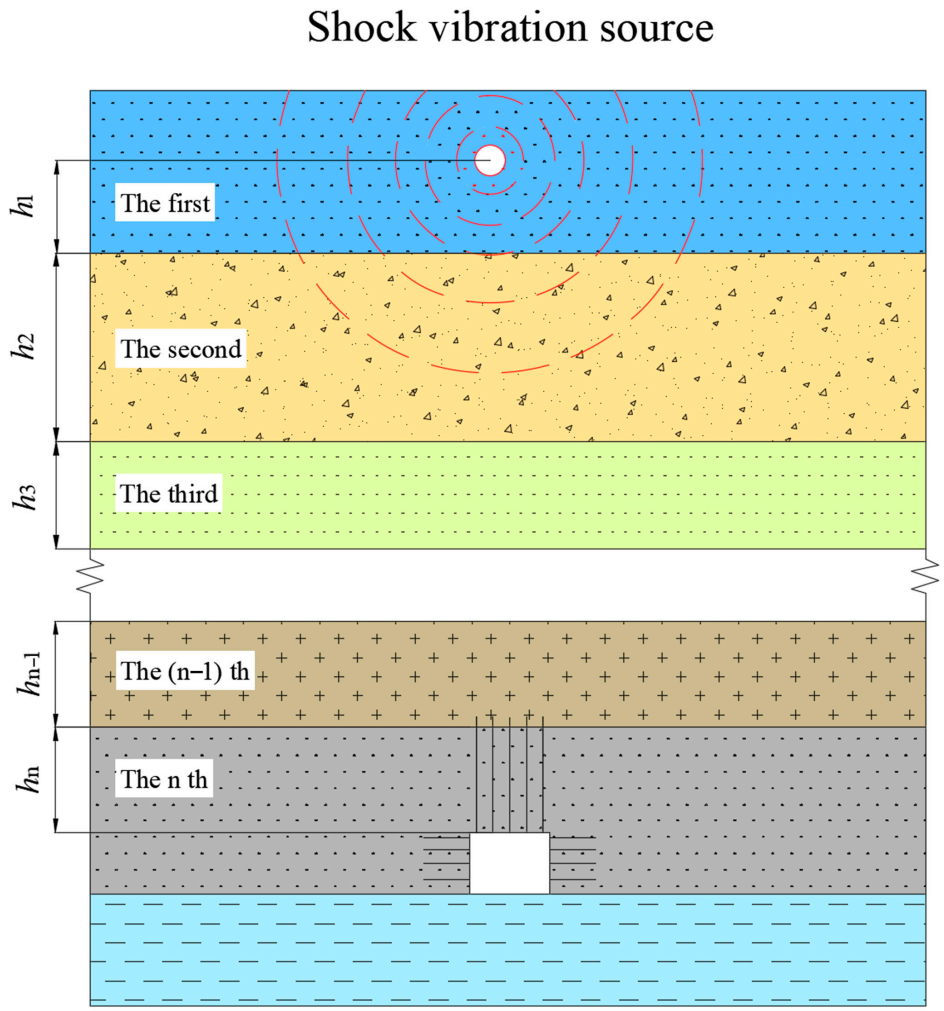


Figure 12. Mechanical modeling of shock wave attenuation through layers.

Compared to large structures such as working faces and chambers, the size and projected area of the roadway section is very small. Simplifying the roadway section to a circular hole, the radial and tangential stresses (σ_r and σ_θ) at the center of the circle for a small hole of radius R in a uniform stress field, according to the theory of elastodynamics, are:

$$\begin{aligned} \sigma_r &= \gamma h\left(1-\frac{r^2}{R^2}\right) \\ \sigma_\theta &= \gamma h\left(1+\frac{r^2}{R^2}\right) \end{aligned} \tag{2}$$

where r is the distance from the center of the circle, and the total distance $h = \sum_{i=1}^{n} h_i$ from the shock source to the roadway where the mine tremor occurs is compared with the radius r of the roadway excavated to satisfy $h \gg r$. Usually, these two physical quantities differ by one to two orders of magnitude. At the same time, the shock wave will fracture and break the rock layer in the process of transmission, and the mine seismic energy will be continuously attenuated; here, the attenuation coefficient of each layer of rock layer is set as η_n. To simplify the study, here, we set the overall lithology of the rock formation as a homogeneous, isotropic rock, while ignoring creep and the viscous characteristics of the rock, and simplify it to a planar model for analytical solution.

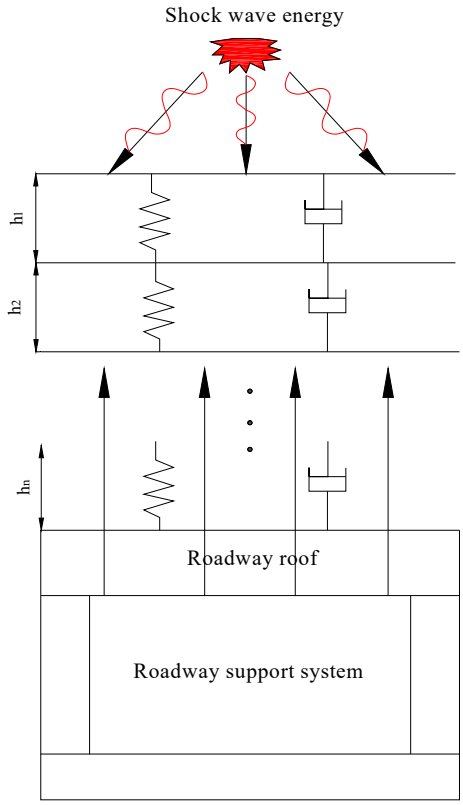


Figure 13. Simplification of the model.

Figure 13 shows the simplified form of the shock wave penetration decay model. The shock energy wave penetrates the top plate of n layers in turn to reach the location of the roadway, and acts on the roadway envelope to produce the damage effect. Here, we set the impact intensity at the source to be σ_{d}. Assuming there is no delamination between rock formations, there is no stress or energy loss when the dynamic wave passes between the formations. When the shock wave penetrates the first formation of rock, according to the propagation characteristics and energy attenuation characteristics in the elastomeric medium, it is known that the intensity of the shock wave arriving at the second formation is as follows:

$$\sigma_A = \sigma_{\mathrm{d}} \cdot {h_1}^{-\eta_1} \tag{3}$$

Therefore, it can be recursively obtained that when the shock wave reaches the roadway, the impact strength of the surrounding rock is as follows:

$$\sigma_{h_n} = \sigma_A \cdot \prod_{i=1}^{n} {h_i}^{-\eta_i} \tag{4}$$

When the shock wave is transmitted to the vicinity of the roadway support system, the shock wave, the surrounding rock endowment stress and the roadway support system interact with each other. Assuming that the shock source is located directly above the roadway roof, the resulting shock pressure will mainly act on the roadway roof in the form of radial stress. As the above research shows, the support strength of the anchor cable combined with the strength of the roof resists the damage of the shock wave. The shock transferred to the support system, the surrounding rock's stresses superimposed on each other and the roadway roof's own impact strength and support strength coupling balance; if the roadway can resist the impact load, then the following conditions will be met:

$$\sigma_{h_n} + \sigma_r \leq \sigma_s + \sigma_c \tag{5}$$

where σ_s is the maximum bearing stress of the support system of the roadway roof and σ_0 is the impact strength of the rock layer of the roadway roof itself. Bringing Equation (1) and Equation (3) into Equation (4), the following can be obtained:

$$\sigma_A \cdot \prod_{i=1}^{n} {h_i}^{-\eta_i} + \gamma h\left(1 - \frac{r^2}{R^2}\right) \leq \sigma_s + \sigma_c \tag{6}$$

Since the calculation here is the surrounding rock force of the roadway support body system, the strength balance position calculated here is between the roadway roof support system and the non-supported body, so the size of R in the equation should be the sum of the anchor length l and the radius r of the roadway, and the left side of Inequality (4) can be converted as follows:

$$\sigma_A \cdot \prod_{i=1}^{n-1} {h_i}^{-\eta_i} + \gamma h\left(1 - \frac{r^2}{(l+r)^2}\right) = \sigma_{h_n} + \sigma_r \tag{7}$$

where l is the length of the longest anchor or cable. When the inequality relationship of Inequality (8) is satisfied, i.e., the strength of the shock wave propagated to the roadway envelope is greater than the impact strength of the roadway envelope and support system, the roadway is damaged. Otherwise, the roadway will be stable. Inequality (8) becomes a criterion for testing whether the roadway will be damaged under the influence of a shock wave.

$$\sigma_A \cdot \prod_{i=1}^{n-1} {h_i}^{-\eta_i} + \gamma h\left(1 - \frac{r^2}{(l+r)^2}\right) \begin{cases} \leq \sigma_s + \sigma_c \\ > \sigma_s + \sigma_c \end{cases} \tag{8}$$

According to the corresponding mechanical model, the attenuation of the stress of the shock wave after passing through the rock formation was analyzed. The attenuation characteristics of the shock wave after passing through the rock layer were analyzed by substituting different rock formations.

The mechanical attenuation parameters associated with this article were obtained through numerical simulations; the attenuation rates of shock waves in actual rock formations were not measured due to equipment factors. In the future, our model can be confirmed by setting up several vibration monitoring probes in the rock formation by certain means.

5. Conclusions

(1) The deformation and damage characteristics of the roadway under the superposition of static and dynamic loads were analyzed in the Hujiahe Coal Mine as a case study.
(2) A numerical simulation model was established based on the production background of the Hujiahe mine, and the transmission characteristics of shock waves in the rock formation were analyzed. The shock wave is continuously attenuated as it passes from the impact shock source to the roadway. The distance between the rock formation and the impact shock source, and the rock properties are the main factors affecting the shock wave attenuation rate.
(3) Based on the results of numerical simulations, a mechanical model of shock wave attenuation through the rock formation was established. An attenuation equation for the shock strength of the shock wave when it passes through the rock formation and reaches the roadway was derived.

Note that it is impossible to set up monitoring stations in every rock formation in the field at present. Furthermore, there is no detailed analysis of the relationship between the axial force of the anchor cable and the stresses in the roadway-surrounding rock, which will be carried out in the future.

Author Contributions: S.Z. conceived the research and wrote the original draft. M.G. revised and reviewed the manuscript. D.X. and X.Y. were responsible for data curation. H.Z. translated and modified this paper. All authors have read and agreed to the published version of the manuscript.

Funding: This research was funded by the National Natural Science Foundation of China (51564044). The authors thank the Hujiahe Coal Mine for their support during the field test.

Institutional Review Board Statement: Not applicable.

Informed Consent Statement: Not applicable.

Data Availability Statement: The data used to support the findings of this study are available from the corresponding author upon request.

Conflicts of Interest: The authors declare no conflict of interest.

References

1. Li, T.; Cai, M.F.; Cai, M. A review of mining-induced seismicity in China. *Int. J. Rock Mech. Min. Sci.* **2007**, *44*, 1149–1171. [CrossRef]
2. Ghorbani, M.; Shahriar, K.; Sharifzadeh, M.; Masoudi, R. A critical review on the developments of rock support systems in high stress ground conditions. *Int. J. Min. Sci. Technol.* **2020**, *30*, 555–572. [CrossRef]
3. Junfeng, P.; Shuwen, W.; Hang, L.; Taotao, D. The Theory and Technology System to Preventing Rock Burst in Mining and Tunneling Space. In *Proceedings of 2015 International Symposium—Safety and High Efficiency Mining in Coal*; Qi, Q., Kang, H., Kuek, M., Eds.; St Plum-Blossom Press Pty Ltd.: Hawthorn East, Australia, 2015; pp. 125–136.
4. Ma, T.-H.; Tang, C.-A.; Liu, F.; Zhang, S.-C.; Feng, Z.Q. Microseismic monitoring, analysis and early warning of rockburst. *Geomat. Nat. Hazards Risk* **2021**, *12*, 2956–2983. [CrossRef]
5. Xue, R.; Liang, Z.; Xu, N. Rockburst prediction and analysis of activity characteristics within surrounding rock based on microseismic monitoring and numerical simulation. *Int. J. Rock Mech. Min. Sci.* **2021**, *142*, 104750. [CrossRef]
6. Zhang, S.; Tang, C.; Wang, Y.; Li, J.; Ma, T.; Wang, K. Review on Early Warning Methods for Rockbursts in Tunnel Engineering Based on Microseismic Monitoring. *Appl. Sci.* **2021**, *11*, 10965. [CrossRef]
7. Chen, X.; Li, L.; Wang, L.; Qi, L. The current situation and prevention and control countermeasures for typical dynamic disasters in kilometer-deep mines in China. *Saf. Sci.* **2019**, *115*, 229–236. [CrossRef]
8. Zhou, J.; Li, X.; Mitri, H.S. Evaluation method of rockburst: State-of-the-art literature review. *Tunn. Undergr. Space Technol.* **2018**, *81*, 632–659. [CrossRef]
9. Gao, M.-S.; Dou, L.-M.; Xie, Y.-S.; Gao, J.; Zhang, L.-S. Latest progress on study of stability control of roadway surrounding rocks subjected to rock burst. *Procedia Earth Planet. Sci.* **2009**, *1*, 409–413. [CrossRef]
10. Sainoki, A.; Emad, M.Z.; Mitri, H.S. Study on the efficiency of destress blasting in deep mine drift development. *Can. Geotech. J.* **2017**, *54*, 518–528. [CrossRef]
11. Afraei, S.; Shahriar, K.; Madani, S.H. Statistical analysis of rock-burst events in underground mines and excavations to present reasonable data-driven predictors. *J. Stat. Comput. Simul.* **2017**, *87*, 3336–3376. [CrossRef]
12. Cui, Z.; Chanda, E.; Zhao, J.; Wang, Z. Stress distribution characteristics in the vicinity of coal seam floor. In *Proceedings of the 2017 3rd International Conference on Environmental Science and Material Application (esma2017), Vols 1–4*; Iop Publishing Ltd.: Bristol, UK, 2008; Volume 108, p. 032056. [CrossRef]
13. Li, Y.; Zhou, C. Rockburst Inducement Mechanism and Its Prediction Based on Microseismic Monitoring. *Geofluids* **2021**, *2021*, 4028872. [CrossRef]
14. Di, Y.; Wang, E. Rock Burst Precursor Electromagnetic Radiation Signal Recognition Method and Early Warning Application Based on Recurrent Neural Networks. *Rock Mech. Rock Eng.* **2021**, *54*, 1449–1461. [CrossRef]
15. Feng, G.; Lin, M.; Yu, Y.; Fu, Y. A Microseismicity-Based Method of Rockburst Intensity Warning in Deep Tunnels in the Initial Period of Microseismic Monitoring. *Energies* **2020**, *13*, 2698. [CrossRef]
16. Zhang, M.; Jiang, F. Rock burst criteria and control based on an abutment-stress-transfer model in deep coal roadways. *Energy Sci. Eng.* **2020**, *8*, 2966–2975. [CrossRef]
17. Gao, M.; He, Y.; Xu, D.; Yu, X. A New Theoretical Model of Rock Burst-Prone Roadway Support and Its Application. *Geofluids* **2021**, *2021*, 5549875. [CrossRef]
18. Wang, Z.-Y.; Dou, L.-M.; Wang, G.-F. Mechanism Analysis of Roadway Rockbursts Induced by Dynamic Mining Loading and Its Application. *Energies* **2018**, *11*, 2313. [CrossRef]
19. Cai, W.; Bai, X.; Si, G.; Cao, W.; Gong, S.; Dou, L. A Monitoring Investigation into Rock Burst Mechanism Based on the Coupled Theory of Static and Dynamic Stresses. *Rock Mech. Rock Eng.* **2020**, *53*, 5451–5471. [CrossRef]
20. Gao, M.-T.; Song, Z.-Q.; Duan, H.-Q.; Xin, H.-Q.; Tang, J.-Q. Mechanical Properties and Control Rockburst Mechanism of Coal and Rock Mass with Bursting Liability in Deep Mining. *Shock Vib.* **2020**, *2020*, 8833863. [CrossRef]
21. Lu, Z.; Ju, W.; Gao, F.; Feng, Y.; Sun, Z.; Wang, H.; Yi, K. A New Bursting Liability Evaluation Index for Coal—The Effective Elastic Strain Energy Release Rate. *Energies* **2019**, *12*, 3734. [CrossRef]

22. Lu, Z.; Ju, W.; Gao, F.; Yi, K. Influence of Loading Rate on the Failure Characteristics of Composite Coal-Rock Specimens Under Quasi-static Loading Conditions. *Rock Mech. Rock Eng.* **2022**, *55*, 909–921. [CrossRef]
23. Dai, L.; Pan, Y.; Li, Z.; Wang, A.; Xiao, Y.; Liu, F.; Shi, T.; Zheng, W. Quantitative mechanism of roadway rockbursts in deep extra-thick coal seams: Theory and case histories. *Tunn. Undergr. Space Technol.* **2021**, *111*, 103861. [CrossRef]
24. Li, L.; Zhang, H.; Pan, Y.; Ju, X.; Tang, L.; Li, M. Influence of stress wave-induced disturbance on ultra-low friction in broken blocks. *Int. J. Coal Sci. Technol.* **2022**, *9*, 22. [CrossRef]
25. Gao, F.; Stead, D.; Kang, H. Numerical Simulation of Squeezing Failure in a Coal Mine Roadway due to Mining-Induced Stresses. *Rock Mech. Rock Eng.* **2015**, *48*, 1635–1645. [CrossRef]
26. Guo, G.; Kang, H.; Qian, D.; Gao, F.; Wang, Y. Mechanism for Controlling Floor Heave of Mining Roadways Using Reinforcing Roof and Sidewalls in Underground Coal Mine. *Sustainability* **2018**, *10*, 1413. [CrossRef]
27. Zheng, C.; Zheng, J.; Peng, X.; Zhou, L. Study on Failure Characteristics and Rock Burst Mechanism of Roadway Roof under Cyclic Dynamic Load. *Shock Vib.* **2021**, *2021*, 7074350. [CrossRef]
28. Gao, M.; Zhao, Y.; Chen, X.; Lu, Q.; Liu, A. Destruction mechanism of rock burst in mine roadways and their prevention. *Disaster Adv.* **2013**, *6*, 34–43.
29. Yun-liang, T.; Ze, Z.; Chuan-le, M. Rock Burst Disaster induced by Mining Abutment Pressure. *Disaster Adv.* **2012**, *5*, 378–382.
30. Wang, P.; Zhang, N.; Kan, J.; Xu, X.; Cui, G. Instability Mode and Control Technology of Surrounding Rock in Composite Roof Coal Roadway under Multiple Dynamic Pressure Disturbances. *Geofluids* **2022**, *2022*, 8694325. [CrossRef]
31. Yan, H.; Deng, X.; Fang, K.; Guo, S.; Li, W. Roof Catastrophe Mechanism of Roadways with Extra-thick Coal Seam and its Controlling Countermeasures. *Disaster Adv.* **2013**, *6*, 236–243.

Disclaimer/Publisher's Note: The statements, opinions and data contained in all publications are solely those of the individual author(s) and contributor(s) and not of MDPI and/or the editor(s). MDPI and/or the editor(s) disclaim responsibility for any injury to people or property resulting from any ideas, methods, instructions or products referred to in the content.